Structural and Ferroelectric Transition in Few-Layer HfO_2 Films by First Principles Calculations

Ruiling Gao(高瑞灵)[1], Chao Liu(刘超)[2,1], Bowen Shi(施博文)[3,1], Yongchang Li(李永昌)[1], Bing Luo(罗兵)[1], Rui Chen(陈睿)[1], Wenbin Ouyang(欧阳文彬)[1], Heng Gao(高恒)[1], Shunbo Hu(胡顺波)[1,4*], Yin Wang(王音)[1,5], Dongdong Li(李东栋)[6*], and Wei Ren(任伟)[1*]

[1]*Materials Genome Institute, State Key Laboratory of Advanced Special Steel, Shanghai Key Laboratory of High Temperature Superconductors, International Center of Quantum and Molecular Structures, Physics Department, Institute for the Conservation of Cultural Heritage, Shanghai University, Shanghai 200444, China*
[2]*Hefei National Research Center for Physical Sciences at the Microscale, University of Science and Technology of China, Hefei 230026, China*
[3]*Shanghai World Foreign Language Academy, Shanghai 200233, China*
[4]*Key Laboratory of Silicate Cultural Relics Conservation (Ministry of Education), Shanghai University, Shanghai 200444, China*
[5]*Hongzhiwei Technology (Shanghai) Co., Ltd., Shanghai 201206, China*
[6]*Zhangjiang Laboratory, Shanghai 201210, China*

(Received 2 April 2024; accepted manuscript online 9 July 202)

The discovery of ferroelectricity in HfO_2-based materials with high dielectric constant has inspired tremendous research interest for next-generation electronic devices. Importantly, films structure and strain are key factors in exploration of ferroelectricity in fluorite-type oxide HfO_2 films. Here we investigate the structures and strain-induced ferroelectric transition in different phases of few-layer HfO_2 films (layer number $N = 1$–5). It is found that HfO_2 films for all phases are more stable with increasing films thickness. Among them, the $Pmn2_1$ (110)-oriented film is most stable, and the films of $N = 4$, 5 occur with a $P2_1$ ferroelectric transition under tensile strain, resulting in polarization about 11.8 $\mu C/cm^2$ along in-plane a-axis. The ferroelectric transition is caused by the strain, which induces the displacement of Hf and O atoms on the surface to non-centrosymmetric positions away from the original paraelectric positions, accompanied by the change of surface Hf–O bond lengths. More importantly, three new stable HfO_2 2D structures are discovered, together with analyses of computed electronic structures, mechanical, and dielectric properties. This work provides guidance for theoretical and experimental study of the new structures and strain-tuned ferroelectricity in freestanding HfO_2 films.

DOI: 10.1088/0256-307X/41/8/087701

Although traditional ferroelectric perovskites may have excellent ferroelectric properties, their integration to complementary metal oxide semiconductors (CMOS) is poor for the microelectronic devices. On the other hand, the good compatibility with CMOS and existence of ferroelectricity in thin films of HfO_2-based materials have attracted extensive research interest since the discovery of ferroelectricity in Si-doped HfO_2 films in 2011.[1–3] The similar ferroelectric behavior has also been observed in other element-doped HfO_2 films, such as doped by Y,[4] Al,[5,6] Zr,[7,8] Gd,[9,10] La,[11] and Lu.[12] In literature, a great deal of works were published on the ferroelectric phase ($Pca2_1$,[13,14] $Pmn2_1$,[15] $R3m$,[16,17] and $R3$[18]) and on the ferroelectric origin (doping[14,19] and strain[17,20,21]) of HfO_2-based materials. However, there is still unsolved controversy about the physical mechanism of ferroelectricity.

For research of HfO_2 ferroelectric phase, Huan *et al.* systematically predicted its five ferroelectric phases in theory.[22] The $Pca2_1$ and $Pmn2_1$ orthorhombic phases were considered as possible ferroelectric phases of HfO_2 because of their lower free energies and appropriate polarization reversal barriers. Many experimental and theoretical studies reported that the $Pca2_1$ HfO_2 is possible ferroelectric phase.[21,23,24] Until 2018, Wei *et al.* experimentally found that $Hf_{0.5}Zr_{0.5}O_2$ (001)-oriented film exhibited a large ferroelectric polarization (34.0 $\mu C/cm^2$), and the structural characterization revealed an $R3m$ rhombohedral phase rather than the $Pca2_1$ orthorhombic phase.[16] However, Qi *et al.* theoretically showed that the in-plane shear strain on $Hf_{0.5}Zr_{0.5}O_2$ films by $La_{0.7}Sr_{0.3}MnO_3/SrTiO_3$ substrates induced lattice distortion, resulting in the formation of the $Pmn2_1$ polar phase and ferroelectricity.[15] It turns out that the structure[25] and strain are crucial factors for the emergence of ferroelectricity in HfO_2 films.

In this work, we systematically investigate the structure and strain effect in the HfO_2 film ($N = 1$–5) for seven phases. The $Pmn2_1$ (110)-oriented film was found to be most stable, which is different from that of its bulk material in which the Hf atoms for the same c-axis direction

*Corresponding authors. Email: renwei@shu.edu.cn; lidd@zjlab.ac.cn; shunbohu@shu.edu.cn
© 2024 Chinese Physical Society and IOP Publishing Ltd

have a certain offset. More importantly, the $P2_1$ ferroelectric transition was observed in the $Pmn2_1$ (110)-oriented films for $N = 4, 5$ under tensile strain, causing polarization about 11.8 $\mu C/cm^2$ along a-axis. Meanwhile, three new obtained HfO_2 2D structures were stable by checking the phonon dispersion spectrum. In addition, the electronic structure, dielectric properties and mechanical properties of the obtained above new 2D structures were also studied. Our work provides some insights into the study of structures and strain-tuned ferroelectricity in the HfO_2 film.

Here, we firstly studied different films of HfO_2 different phases, and obtained the films of relatively lower energy $Pmn2_1$ (110)-oriented. Then, we focus on the ferroelectric transition of films $Pmn2_1$ (110)-oriented under strain. Finally, we discovered some novel and stable low-dimensional film structures of HfO_2 during the research process, and calculated their electronic structures and mechanical properties.

Methods. Our first-principles calculations were performed by using the projected augmented-wave method [26] as implemented in the Vienna *ab initio* simulation package (VASP) [27] and DS-PAW software [26]. The generalized gradient approximation of Perdew–Burke–Ernzerhof type was employed to treat the exchange-correlation interaction. [28] A vacuum buffer space of 20.0 Å was used to prevent coupling between the two adjacent slabs. The kinetic energy cutoff was set to 450.0 eV. During the full structure relaxation, all atoms and lattice were allowed to relax until the Hellmann–Feynman force on each atom is less than 0.01 eV/Å. In order to understand the properties of the film close to the bulk structure, we also used a fixed-ab way to optimize the film, which cannot fully demonstrate the properties of the film, because it is equivalent to applying a certain strain to the film. For the structural relaxation of fixed-ab lattices, all atoms were allowed to relax but with the lattice fixed. Regardless of the optimization way, we keep the symmetry unchanged during the film structure relaxation. The Brillouin-zone integrations of the other phases except for the $Pmn2_1$ were carried out by using $5 \times 5 \times 1$ for the geometry optimization and $7 \times 7 \times 1$ for the total energy at Monkhorst–Pack k-point meshes. The $9 \times 5 \times 1$ and $11 \times 7 \times 1$ Monkhorst–Pack k-point meshes were used for geometry optimization and total energy calculations in the $Pmn2_1$ film, respectively. Unless otherwise specified, the spin-orbit coupling (SOC) is not considered in the calculation. The phonon dispersion curves were calculated by the Phonopy code [29] with a $2 \times 2 \times 1$ k-mesh using the finite displacement method for a supercell of $3 \times 3 \times 1$ for $Pmn2_1$ (110)-oriented and $P4_2/nmc$ (001)-oriented slabs, but a supercell of $4 \times 4 \times 1$ for $P2_1/c$ (100)-oriented. Here, $Pmn2_1$ (110)-oriented film is cut from the $Pmn2_1$ bulk along the (110) orientation. The ferroelectric polarization using the Berry phase method, [30] dielectric constant, mechanical properties and the band structures of new 2D structures was calculated by employing DS-PAW software. The electronic properties of spin texture are calculated by the Pyprocar [31] code.

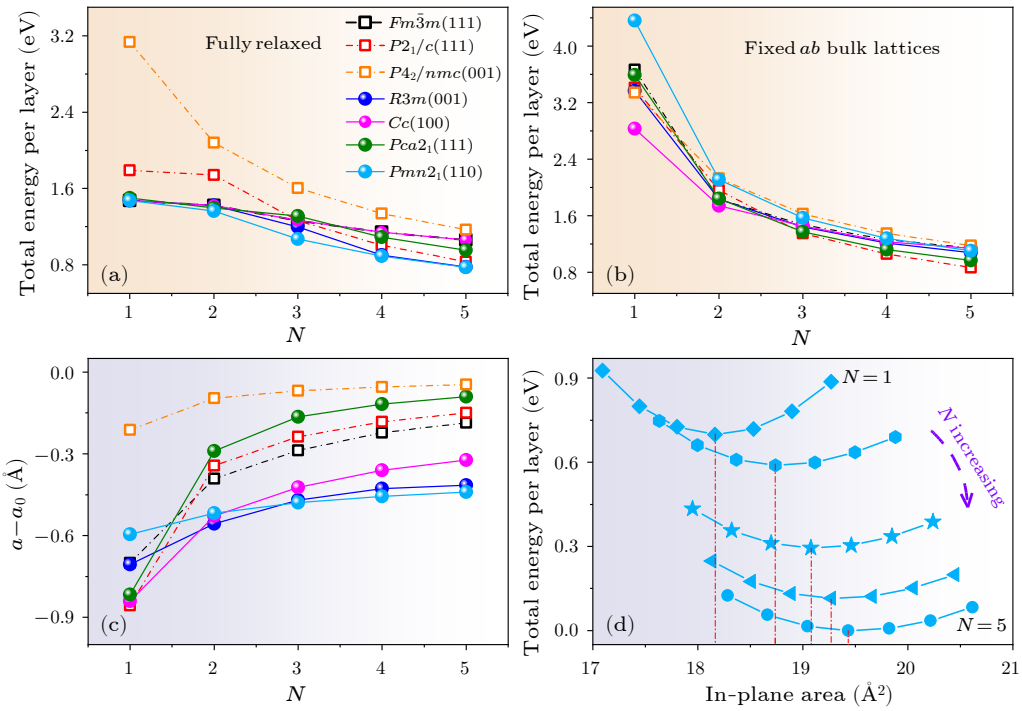

Fig. 1. Total energies of different phases of HfO_2 films per Hf–O_2 layer (two Hf and four O atoms) for two different calculation settings, (a) fully relaxed and (b) fixed-ab bulk lattices. The total energy of strain-free bulk $P2_1/c$ HfO_2 per six atoms is set to be zero. (c) The variation of the lattice constant increment $(a - a_0)$ as a function of films thickness for different phases of HfO_2 films. (d) Total energies of $Pmn2_1$ (110)-oriented HfO_2 film of different thickness (per six atoms) under in-plane biaxial strain. The total energy of strain-free $Pmn2_1$ (110)-oriented HfO_2 film per six atoms at $N = 5$ is set to be zero. The open and solid symbols denote paraelectric and ferroelectric phases of HfO_2, respectively.

Results and Discussion. In 2014, Huan *et al.* reported the eleven lowest-energy structural phases of HfO_2 using the structure search method, including six nonpolar ($P2_1/c$ and $P2_1/m$ monoclinic, $P4_2/nmc$ tetragonal, $Pbca$ and $Pnma$ orthorhombic, and $Fm\bar{3}m$ cubic phases) and five polar phases ($Pca2_1$ and $Pmn2_1$ orthorhombic, Pm and Cc monoclinic, and $P1$ triclinic phases).[22] It was found that ferroelectric phase of HfO_2 might be the $Pca2_1$ and $Pmn2_1$ orthorhombic phases. Later, another possible ferroelectric phase of $R3m$ rhombohedral HfO_2 was experimentally found in 2018.[16] Therefore, we have chosen four possible ferroelectric phases ($Pca2_1$, $Pmn2_1$, $R3m$, and Cc) and three nonpolar phases ($P2_1/c$, $P4_2/nmc$, and $Fm\bar{3}m$). Various HfO_2 phases are constructed with O-terminated and stoichiometric structures as reported to be more stable compared to other configurations,[32] which can also obtain from relatively lower surface energy of Table S1 in the Supplementary Material. The films of different thickness (N) were studied, where N is defined by Hf2–O4 stoichiometric ratio. As shown in Fig. 1(a), we firstly investigated the films stability of the above-mentioned phases at different thicknesses, and the $Pmn2_1$ (110)-oriented film was found to be the most stable in all films thickness in the fully relaxed results. However, Fig. 1(b) shows the variation of energy with film thickness for the fixed-ab case, in which the $P2_1/c$ (111)-oriented film was more stable. We analyzed the lattice constant increment of all systems based on bulk lattices as a function of the film thickness in Fig. 1(c). It was found that the lattice constant increases with the film thickness in both nonpolar and polar phases, which is consistent with the theoretical[17] and experimental[16] results. It is attributed to the size effect of films, in which the surface energy (σ) can produce large internal pressures in nanoparticles of radius (r) according to the formula of $P = 2\sigma/r$. In addition, Fig. 1(d) shows the estimated energy variation upon changing the in-plane area of the $Pmn2_1$ (110)-oriented films for the corresponding different thickness. It is seen that the thicker films are more stable and have larger in-plane areas under the considered strains, which is in good agreement with the results of Fig. 1(c).

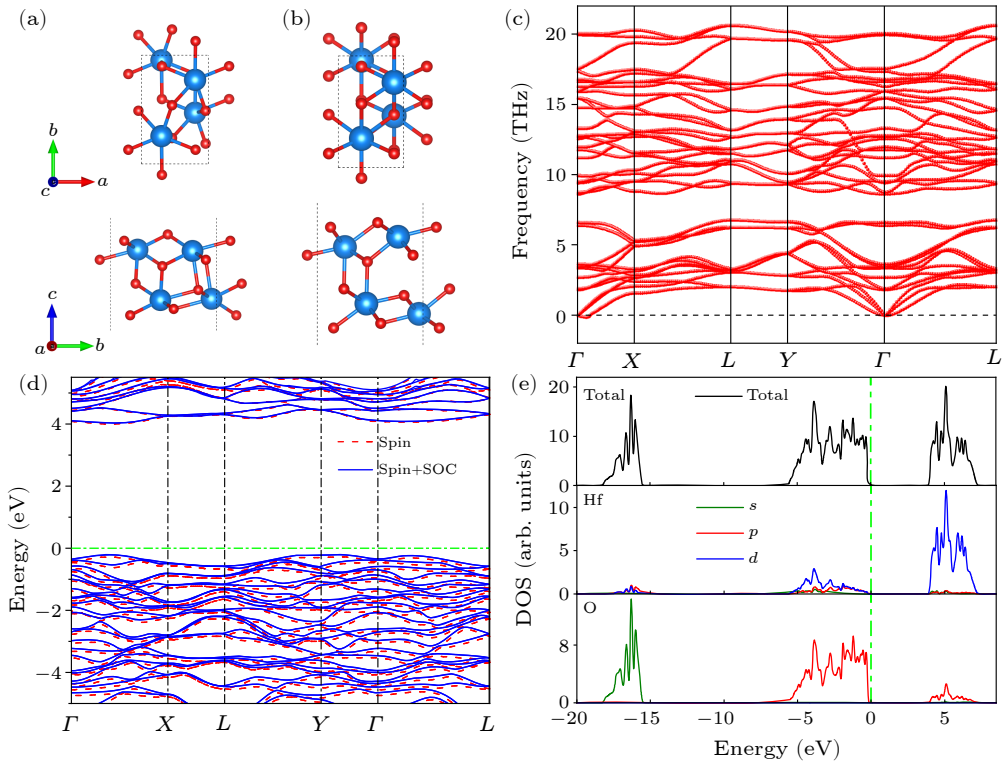

Fig. 2. The $Pmn2_1$ (110)-oriented HfO_2 film with thickness $N = 2$. The schematic illustrations of (a) unrelaxed and (b) fully relaxed structures. (c) The calculated phonon dispersion spectra of fully relaxed structure. (d) The band structures without (red) or with (blue) spin-orbit coupling (SOC). (e) Total density of states (DOS) and projected density of states (PDOS) for the different orbitals of Hf and O elements.

For the $Pmn2_1$ (110)-oriented films with thickness $N = 2$, the schematics of unrelaxed structure similar to the bulk and the fully relaxed structure are shown in Figs. 2(a) and 2(b), respectively. Through a comparison between the fully relaxed and the unrelaxed structure, there is the relative displacement for the original same c-axis direction Hf atoms, meanwhile the lattice constant is reduced and the space group changes from polar $P2_1$ to nonpolar $P2_1/m$. The numerical calculation shows that the energy of the fully relaxed structure is 2.2 eV/4 f.u. lower than that of the unrelaxed. At the same time, we use the density functional perturbation theory to calculate the phonon disper-

sion curve of the fully relaxed structure and proved that it is dynamically stable, as shown in Fig. 2(c). It is seen that most of the frequencies in the first Brillouin zone are positive, and only a very small imaginary frequency exists near Γ point, which can be ignored within the numerical noise,[33] and even completely eliminated.[34] In addition, to discuss its electronic structure, Fig. 2(d) shows the band structures with or without spin-orbit coupling (SOC). Similar to the bulk property, it remains insulating regardless of whether the SOC is considered. Compared with no SOC, the band gap is reduced by 29.3 meV in the case of SOC, and other features like indirect band gap have not changed significantly. Meanwhile, we report the total density of states (DOS) and projected density of states (PDOS) contributed by the Hf and O elements different orbitals in Fig. 2(e). The contribution to the DOS from Hf atoms comes from the 5p and 5d electrons, whereas the 2s and 2p electrons of O atoms contribute. The total DOS is composed of two valence bands, a lower narrow band lying at about −15.6 eV constituted of mainly O-2s states and another upper band lying between −5.5 and −0.3 eV mainly arising from O 2p states, with a significant conduction band contribution of the Hf 5d orbitals. In addition, the upper valence band is separated by the band gap of 4.27 eV from a conduction band composed of Hf 5d character, which is in agreement with previous theoretical studies.[32,35,36] This reveals that the valence band mainly consists of symmetry O 2p nonbonding orbitals while the conduction band is primarily Hf-5d-like nonbonding orbitals.[32,36] However, our calculations show that the upper valence band exhibits mixing of the O 2p and Hf 5d states, indicating covalence of the Hf–O bonds. In addition, the fully relaxed structures of HfO_2 for other different phase films under different thicknesses are shown in Figs. S1–S7 in the Supplementary Material.

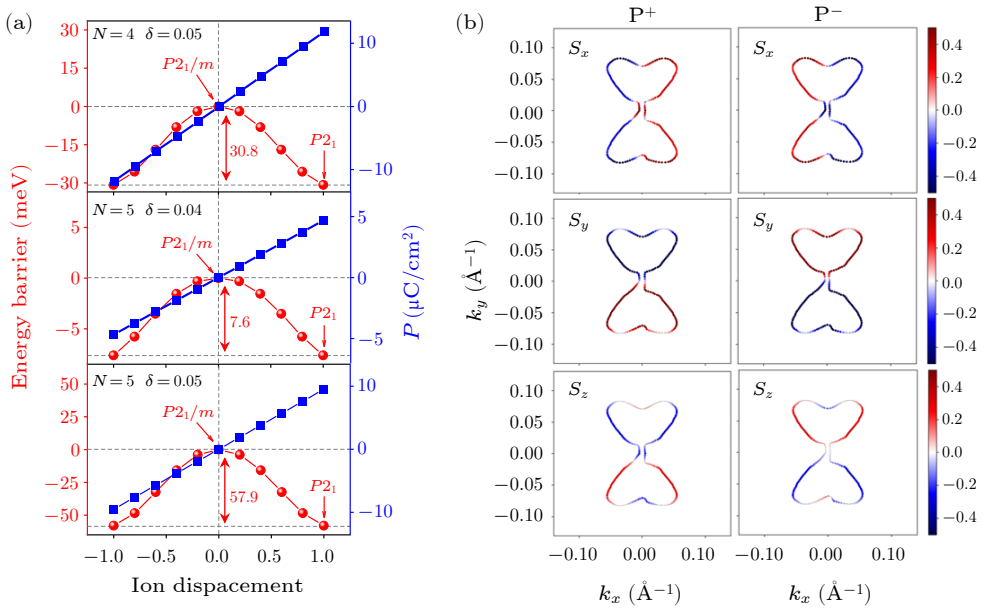

Fig. 3. (a) Variation of energy barrier and ferroelectric polarization versus the ion displacement for different thickness and strain of the HfO_2 films cut from $Pmn2_1$ bulk along the (110) orientation. (b) Spin textures of different polarization directions (thickness $N = 5$, tensile strain $\delta = 0.05$) for the valence band at −0.315 and −0.257 eV for P^+ and P^-.

The strain is one of the key factors for the emergence of HfO_2 ferroelectricity. Therefore, we investigate the effect of strain on the ferroelectricity of the most stable $Pmn2_1$ (110)-oriented HfO_2 films. In our calculations, the application of biaxial strain is achieved by changing the in-plane lattice constant. The strain is applied according to the formula $\delta = (x - x_0)/x_0$ ($x = a, b$), so δ is positive and negative implying tensile and compressive strain. Surprisingly, ferroelectric polarization induced by tensile strain in the $Pmn2_1$ (110)-oriented HfO_2 films is discovered. As shown in Fig. 3(a), HfO_2 films of $N = 5$ presents a ferroelectric transition from nonpolar $P2_1/m$ to polar $P2_1$ at the 0.04 and 0.05 strain, as well as in the film of $N = 4$ under 0.05 strain. Among them, the film of $N = 4$ exhibits 11.8 μC/cm^2 ferroelectric polarization along a-axis under $\delta = 0.05$ strain, and has an inversion barrier of 30.8 meV/8 f.u. The film for $N = 5$ exhibits 4.7 and 9.5 μC/cm^2 ferroelectric polarization along a-axis under 0.04 and 0.05 strain, and has the inversion barrier of 7.6 and 57.9 meV/10 f.u. The emergence of ferroelectric transition is mainly attributed to surface effects, which we will discuss below. It has been found that the ferroelectric polarization can control the spin texture of the ferroelectric material GeTe.[37–39] It is possible for the tuned ferroelectric polarization by an external electric field to regulate the spins states, which has important applications in the spin field effect transistors. Thence, we also study the effect of ferroelectric polarization on the spin texture of the

HfO_2 films. Figure 3(b) shows the spin texture along different directions of the $Pmn2_1$ (110)-oriented HfO_2 films of $N = 5$ under $\delta = 0.05$ strain in the ferroelectric bi-stables, P^+ and P^-. Similar to GeTe, we find that ferroelectric polarization direction inversion can flip the corresponding spin-polarization projection no matter whether it is k_x, k_y or k_z direction. Therefore, spintronics from HfO_2-based ferroelectric materials can also be designed by manipulating the ferroelectric polarization.

To further understand the strain-induced ferroelectric transition mentioned above, we have carefully studied the bond length and charge density under strain. As shown in Fig. 4(a), the upper and lower panels show that the Hf–O bond changes with strain at the surfaces of the $Pmn2_1$ (110)-oriented HfO_2 films of $N = 4$ and $N = 5$, respectively. Among them, Hf1–O1 and Hf1–O2 are defined as the bond lengths of the outermost and inner layers of Hf atoms on the upper surface of the film, respectively. Similarly, Hf2–O1 and Hf2–O2 correspond to the outermost and inner layers of Hf atoms, respectively, on the lower surface. It can be seen that when the strain δ is less than 0.05, the Hf–O bonds of the outermost layers (Hf1–O1 and Hf2–O1) on the upper and lower surfaces of HfO_2 films at $N = 4$ increase with the increase of strain, while the Hf–O bonds of the inner layers (Hf1–O2 and Hf2–O2) remain basically unchanged. However, when $\delta = 0.05$ tensile strain is applied, the bond lengths of the inner and outer Hf–O bonds have a drastic increase. Of course, the phenomenon also occurs in the $N = 5$ film, but the rapid rise of surface Hf–O bond length is induced by $\delta = 0.04$ strain, smaller than that of $N = 4$ film. Meanwhile, Fig. 4(b) shows the two-dimensional charge densities along the (100) plane of HfO_2 films with $N = 4$ and $N = 5$ under strain-free and $\delta = 0.05$ strain. From comparison with and without strain, there is an obvious charge redistribution for Hf–O atoms on the upper or lower surfaces, which is consistent with the previous bond length analysis results. It can be seen that, in the tensile strained case, the electron density between Hf and O atoms on upper surface becomes depleted compared with that of the strain-free case due to considerable elongation of the Hf–O bonds. Interestingly, the electron density between Hf and O atoms on lower surface becomes overall relatively agglomerated and is to be further studied. Therefore, the strain-induced ferroelectric transition in the film is mainly attributed to displacement of Hf and O atoms on the surface to non-centrosymmetric positions away from the original paraelectric position.

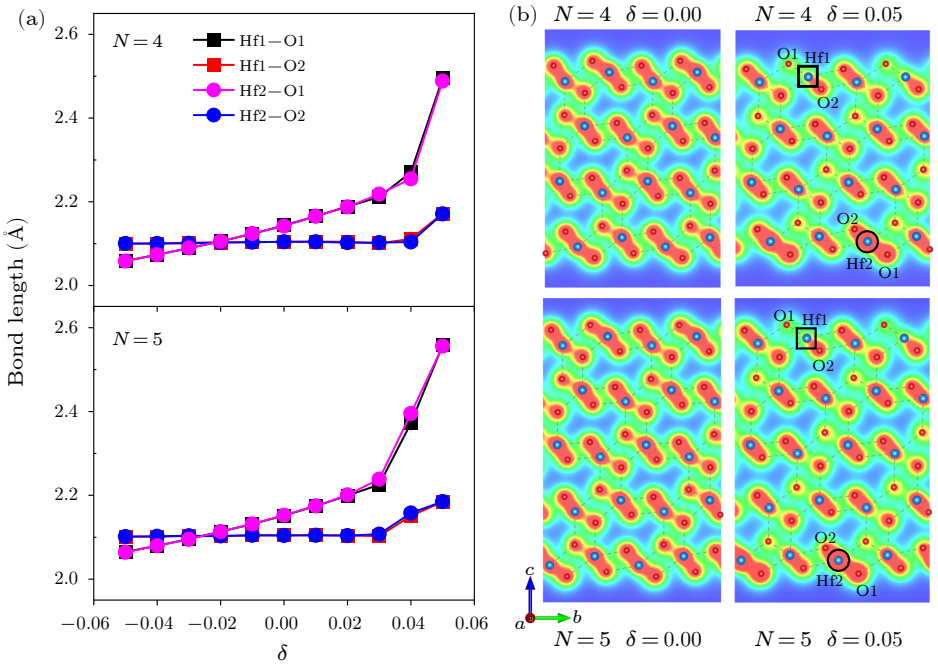

Fig. 4. (a) Hf–O bond length at the upper and lower surfaces of $N = 4$, 5 films as a function of strain. (b) Charge densities along the films (100) plane of the strain-free and biaxially tensile-strained HfO_2.

During the above calculation, the other two new structures of HfO_2 films of tetragonal $P\bar{4}m2$ and monoclinic $P2_1/c$ were found, and their side and top views are shown in Figs. 5(a) and 5(b), respectively. Their lattice constants are listed in Table 1, phonon spectrum calculations are also performed to study their stability, as shown in Fig. 5(c) for $P\bar{4}m2$ film and Fig. 5(d) for $P2_1/c$ film. Most of the frequencies for their phonon dispersion spectra in the first Brillouin zone are positive, and only a very small imaginary frequency exists near Γ point which may be ignored. Meanwhile, it was found that both the new $HfO_2$2D structures have no intrinsic polarization due to their existing spatial inversion symmetry. As shown in Table 1, their cohesive energy is calculated by

$$E_c = [(N_{Hf}E_{Hf} + N_O E_O) - E_{Total}]/(N_{Hf} + N_O),$$

where N_{Hf} and N_O are the numbers of Hf and O atoms in the unit cell, E_{Hf} and E_O denote the energies of the

single Hf and O atoms, and E_{Total} is the total energy of the system. The larger the values of cohesive energy, the higher the relative stability of the system. Compared with the previously reported cohesive energies of HfO_2 2D structures,[25] these three films are more stable due to their larger cohesive energies. Further, the electronic band structures are shown in Fig. S8, which still have the indirect band gaps, about 4.64 eV and 3.60 eV, respectively.

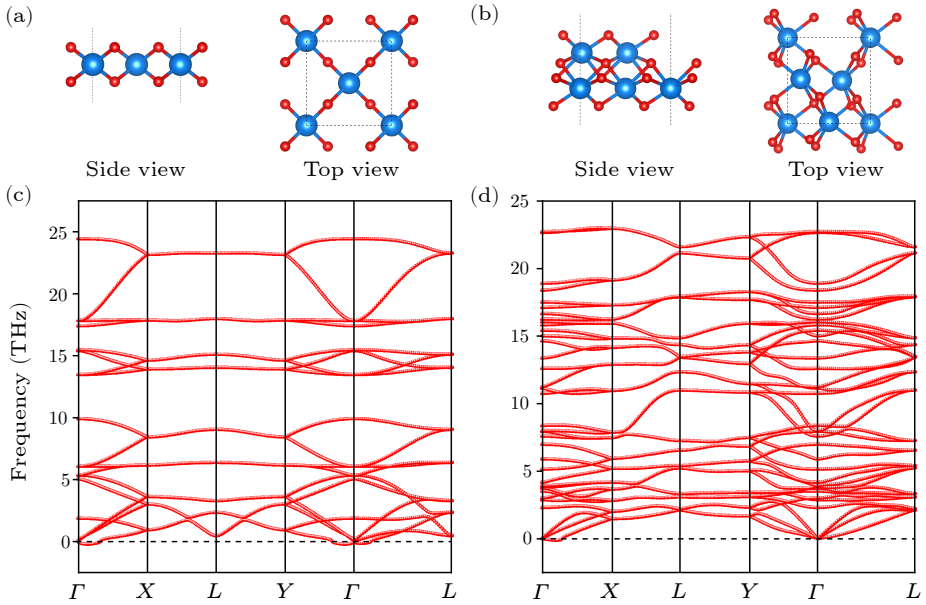

Fig. 5. Schematic structures of other stabilized 2D HfO_2 films from first-principles calculations. (a) Tetragonal $P\bar{4}m2$ monolayer film of $N = 1$, and (b) Monoclinic $P2_1/c$ film of $N = 2$. The corresponding calculated phonon dispersion spectra after relaxation (c) $P\bar{4}m2$ film of $N = 1$, and (b) $P2_1/c$ film of $N = 2$.

In order to study the optical properties of 2D HfO_2, we have investigated its macroscopic static dielectric constants, which include the electronic and ionic contributions to the dielectric response. The macroscopic dielectric tensor of the supercell is calculated, which contains the dielectric response of 2D HfO_2 films. During the calculations, the films not only include 2D crystal structure, but also have a certain vacuum layer in the c direction. Therefore, the static dielectric constant of 2D HfO_2 is calculated according to the following formula:[40,41]

$$\varepsilon_{2\text{D},||} = 1 + \frac{c}{t}(\varepsilon_{\text{sc},||} - 1), \quad \varepsilon_{2\text{D},\perp} = \left[1 + \frac{c}{t}\left(\frac{1}{\varepsilon_{\text{sc},\perp}} - 1\right)\right]^{-1},$$

where $\varepsilon_{2\text{D},||}$ and $\varepsilon_{2\text{D},\perp}$ are the dielectric constants of the supercell corresponding to in-plane and out-of-plane directions, respectively, c is the thickness of the supercell containing the vacuum and 2D HfO_2, and t is the van der Waals effective thickness of 2D HfO_2. Due to the anisotropy of the structure, the dielectric tensors of the x, y directions as well as the out-of-plane directions are calculated, as listed in Table 1. The dielectric responses of these three structures are comparable to the previously reported average dielectric constant values of bulk HfO_2. Therefore, according to the mathematical expression $C = \varepsilon S/4\pi kd$, 2D HfO_2 films with smaller thickness obtain a larger capacitance, which could benefit potential supercapacitors and dielectric layers for advanced nanoscale electronic devices.

To investigate their mechanical stability, we have further calculated the elastic tensor of 2D HfO_2, as shown in Table S2. Based on the Born–Huang criteria,[42,43] the elastic constants of the stable crystal should satisfy $C_{11}C_{22} - C_{12}^2 > 0$ and $C_{66} > 0$. Our numerical calculations show that the predicted 2D HfO_2 structures all also obey the criteria, indicating theoretically the mechanical stability of them. Moreover, other mechanical properties were investigated, including the in-plane Young's modulus and Poisson's ratio, as shown in Table S1. The larger the Young modulus, the better the rigidity of the material and the less likely it is to deform. We verify that 2D HfO_2 tetragonal ($P\bar{4}m2$) is the softest in terms of Young's modulus, which is probably due to the thinner thickness. At the same time, it has good toughness in terms of Poisson's ratio, which can be potentially applied in nanomechanics.

Table 1. Structural parameters and static dielectric constant (ε) of three new stable HfO_2 2D films, with the space groups, lattice parameters, cohesive energy, and band gap. The in-plane ($\varepsilon_{2\text{D},xx}$, $\varepsilon_{2\text{D},yy}$) and out-of-plane ($\varepsilon_{2\text{D},\perp}$) dielectric constants are considered.

Phases	Tetragonal ($P\bar{4}m2$)	Monoclinic-I ($P2_1/c$)	Monoclinic-II ($P2_1/m$)
Lattice constants (Å)	$a = b = 3.43$, $c = 22.04$	$a = 5.19$, $b = 5.34$, $c = 19.38$	$a = 5.63$, $b = 3.31$, $c = 24.69$
Cohesive energy (eV per atom)	7.47	7.54	7.76
Band gap (eV)	4.64	3.60	4.27
$\varepsilon_{2\text{D},xx}$	7.49	7.60	24.53
$\varepsilon_{2\text{D},yy}$	7.49	21.37	22.86
$\varepsilon_{2\text{D},\perp}$	2.65	3.35	3.59

In summary, we have explored the 2D structures and

strain-induced ferroelectric transition of few-layer HfO_2 films using first-principles density functional theory computations. It is found that the $Pmn2_1$ (110)-oriented films of $N = 1$–5 layers are more stable, compared with the films of other phases. Importantly, the $Pmn2_1$ (110)-oriented films of $N = 4$, 5 show an emergence of the $P2_1$ ferroelectric transition under tensile strain, resulting in a polarization along a-axis of about 11.8 $\mu C/cm^2$. The ferroelectric transition has arisen from a rapid change of the upper and lower surface Hf–O bonds in the films. Furthermore, three new nonpolar and stable HfO_2 2D structures are obtained, which all have indirect band gap. The thinner HfO_2 2D films with comparable dielectric tensor to bulk have great potential applications for future nanoscale electronic devices. Our theoretical predictions provide guidance for exploring structures and strain-tuned ferroelectricity of the HfO_2 film, and the design of next-generation ferroelectric random access memories.

Acknowledgments. This work was supported by the National Key R&D Program of China (Grant No. 2023YFB4402600), the National Natural Science Foundation of China (Grant Nos. 12074241, 11929401, 52130204, 12311530675, and 52271007), Key Research Project of Zhejiang Lab (Grant No. 2021PE0AC02), and Science and Technology Commission of Shanghai Municipality (Grant Nos. 22XD1400900, 20501130600, 21JC1402700, and 21JC1402600). H.G. acknowledges the supports from the open projects of Key Laboratory of Green Fabrication and Surface Technology of Advanced Metal Materials (Anhui University of Technology), Ministry of Education (Grant No. GFST2022KF08), State Key Laboratory of Surface Physics (Fudan University) (Grant No. KF2022_10), and State Key Laboratory of Infrared Physics, Shanghai Institute of Technical Physics, Chinese Academy of Sciences (Grant No. SITP-NLIST-YB-2022-08). R.L.G. acknowledgments the support of China Scholarship Council, and thanks Mr. Xiaowen Shi (from HZWTECH) for helpful discussions. We gratefully acknowledge HZWTECH for providing computation facilities.

References

[1] Park M H, Lee Y H, Mikolajick T, Schroeder U, and Hwang C S 2018 *MRS Commun.* **8** 795
[2] Fan Z, Chen J, and Wang J 2016 *J. Adv. Dielectr.* **6** 1630003
[3] Böscke T S, Müller J, Bräuhaus D, Schröder U, and Böttger U 2011 *Appl. Phys. Lett.* **99** 102903
[4] Lee K, Lee T Y, Yang S M, Lee D H, Park J, and Chae S C 2018 *Appl. Phys. Lett.* **112** 202901
[5] Mueller S, Mueller J, Singh A *et al.* 2012 *Adv. Funct. Mater.* **22** 2412
[6] Vulpe S, Nastase F, Dragoman M *et al.* 2019 *Appl. Surf. Sci.* **483** 324
[7] Hyuk Park M, Joon Kim H, Jin Kim Y, Lee W, Moon T, and Seong Hwang C 2013 *Appl. Phys. Lett.* **102** 242905
[8] Lee Y, Kim S H, Jeong H W *et al.* 2024 *Appl. Surf. Sci.* **648** 158948
[9] Mueller S, Adelmann C, Singh A, Van Elshocht S, Schroeder U, and Mikolajick T 2012 *ECS J. Solid State Sci. Technol.* **1** N123
[10] Hoffmann M, Schroeder U, Schenk T *et al.* 2015 *J. Appl. Phys.* **118** 072006
[11] Schroeder U, Richter C, Park M H *et al.* 2018 *Inorg. Chem.* **57** 2752
[12] Tromm T C U, Zhang J, Schubert J *et al.* 2017 *Appl. Phys. Lett.* **111** 142904
[13] Wu J, Zhang Y, Zhang L, and Liu S 2021 *Phys. Rev. B* **103** 024108
[14] Li T, Ye M, Sun Z Z *et al.* 2019 *ACS Appl. Mater. Interfaces* **11** 4139
[15] Qi Y B, Singh S, Lau C *et al.* 2020 *Phys. Rev. Lett.* **125** 257603
[16] Wei Y F, Nukala P, Salverda M *et al.* 2018 *Nat. Mater.* **17** 1095
[17] Zhang Y, Yang Q, Tao L, Tsymbal E Y, and Alexandrov V 2020 *Phys. Rev. Appl.* **14** 014068
[18] Barabash S V 2017 *J. Comput. Electron.* **16** 1227
[19] Park M H, Chung C C, Schenk T *et al.* 2018 *Adv. Electron. Mater.* **4** 1700489
[20] Fan S T, Chen Y W, and Liu C W 2020 *J. Phys. D* **53** 23LT01
[21] Batra R, Huan T D, Jones J L, Rossetti Jr G, and Ramprasad R 2017 *J. Phys. Chem. C* **121** 4139
[22] Huan T D, Sharma V, Rossetti Jr G A, and Ramprasad R 2014 *Phys. Rev. B* **90** 064111
[23] Sang X, Grimley E D, Schenk T, Schroeder U, and LeBeau J M 2015 *Appl Phys Lett.* **106** 162905
[24] Schenk T, Fancher C M, Park M H *et al.* 2019 *Adv. Electron. Mater.* **5** 1900303
[25] Wang Y and Ren J 2020 *Phys. Chem. Chem. Phys.* **22** 4481
[26] Blöchl P E 1994 *Phys. Rev. B* **50** 17953
[27] Kresse G and Furthmüller J 1996 *Phys. Rev. B* **54** 11169
[28] Perdew J P, Chevary J A, Vosko S H *et al.* 1993 *Phys. Rev. B* **48** 4978
[29] Alfè D 2009 *Comput. Phys. Commun.* **180** 2622
[30] Spaldin N A 2012 *J. Solid State Chem.* **195** 2
[31] Herath U, Tavadze P, He X *et al.* 2020 *Comput. Phys. Commun.* **251** 107080
[32] Mukhopadhyay A B, Sanz J F, and Musgrave C B 2006 *Phys. Rev. B* **73** 115330
[33] Wang Z and Zhou G 2020 *J. Phys. Chem. C* **124** 167
[34] Zólyomi V, Drummond N D, and Fal'ko V I 2014 *Phys. Rev. B* **89** 205416
[35] Demkov A A 2001 *Phys. Status Solidi* **226** 57
[36] Sayan S, Emge T, Garfunkel E *et al.* 2004 *J. Appl. Phys.* **96** 7485
[37] Rinaldi C, Varotto S, Asa M *et al.* 2018 *Nano Lett.* **18** 2751
[38] Picozzi S 2014 *Front. Phys.* **2** 10
[39] Di Sante D, Barone P, Bertacco R, and Picozzi S 2013 *Adv. Mater.* **25** 509
[40] Weng J and Gao S P 2018 *Phys. Chem. Chem. Phys.* **20** 26453
[41] Laturia A, Van de Put M L, and Vandenberghe W G 2018 *npj 2D Mater. Appl.* **2** 6
[42] Gao Z, Dong X, Li N, and Ren J 2017 *Nano Lett.* **17** 772
[43] Ding Y and Wang Y 2013 *J. Phys. Chem. C* **117** 18266